NUCLEAR INSTRUMENTS AND METHODS 13 (1961) 70–82; NORTH-HOLLAND PUBLISHING CO.

# THE RESPONSE OF ORGANIC SCINTILLATORS TO FAST NEUTRONS

R. BATCHELOR, W. B. GILBOY, J. B. PARKER and J. H. TOWLE

*Atomic Weapons Research Establishment, Aldermaston, Berks.*

Received 29 April 1961

The pulse height distributions for organic liquid scintillation counters irradiated with fast neutrons have been calculated using a Monte Carlo computer programme. The results obtained at 1, 4 and 14 MeV neutron energies for a cylindrical scintillator 2″ diameter × 2½″ long have been compared with experimental measurements and good agreement is obtained. In the experiments, the pulse shape discrimination and time of flight techniques have been used independently to eliminate the effect of $\gamma$-rays. The neutron detection efficiency has also been measured in the energy range 0.4 to 3.5 MeV and the results compared qualitatively with those obtained by the Monte Carlo calculation. In addition the pulse height response of the liquid scintillator type NE213 for protons and electrons is obtained and this is similar to that of the plastic phosphor type NE102.

## 1. Introduction

Since the discovery that pulses due to protons and electrons from counters employing certain organic scintillators can be distinguished from their shapes[1,2]), the utility of these scintillators has increased considerably. Thus a scintillator with linear dimensions of a few inches can be used as an efficient monitor of fast neutrons in the presence of a fairly intense $\gamma$-ray flux. Several methods have previously been used to reduce the relative efficiency to $\gamma$-rays[3]). For example this can be achieved by restricting the size of the scintillator such that the recoil protons are retained within the material whereas most of the lightly ionising electrons escape[4]). However, this invariably leads to a much reduced efficiency for neutron detection.

Litherland *et al.*[5]) have shown that a cylindrical liquid scintillator of dimensions 1½″ diameter, 1½″ long can also be used as a crude neutron spectrometer in certain cases. They were able to distinguish the neutron groups emitted in the reactions $Be^9(He^4, n)C^{12}$ and $Be^9(He^3, n)C^{11}$. These authors also pointed out the usefulness of the detector, when used in conjunction with a NaI detector, for coincidence measurements between neutrons and $\gamma$-rays emitted in nuclear reactions. Subsequently the idea was demonstrated in a study of (d,n) stripping reactions on $B^{10}$ and $B^{11}$ (ref. [6])).

In view of these developments it is therefore of considerable interest to know the pulse height distributions from these counters when placed in fluxes of monoenergetic neutrons. Such distributions could be used to deduce a neutron spectrum from an observed pulse distribution. Also if the area under each distribution is related theoretically to the incident neutron flux, then unknown neutron intensities can be measured.

This paper reports the results of some Monte Carlo calculations carried out for two cylindrical liquid scintillators, type NE213† 2″ diameter, 2½″ long and 3″ diameter, 4″ long, using the Aldermaston I.B.M. 7090 computer. These calculations, which have been made for incident neutrons of energies 0.7, 1, 2, 4, 8 and 14 MeV, and also for a fission spectrum, take into account all the known important effects which influence output pulse height. Thus, each neutron is tracked through the scintillator until it either escapes or is absorbed by the material. The type of each interaction it makes is catalogued and also the energies imparted to the

† Supplied by Nuclear Enterprises (G.B.) Ltd., Edingburgh.

[1]) F. D. Brooks, Nucl. Instr. and Meth. **4** (1959) 151.

[2]) R. B. Owen, Trans. I.R.E. on Nuclear Sci. NS-5 (1958) 198.

[3]) C. D. Swartz and G. E. Owen, Fast Neutron Physics, Part I (1960) 215.

[4]) J. R. Beyster, R. L. Henkel, R. A. Nobles and J. M. Kister, Phys. Rev. **98** (1955) 1216.

[5]) A. E. Litherland, E. Almqvist, R. Batchelor and H. E. Gove, Phys. Rev. Letters **2**, No. 3 (1959) 511.

[6]) A. J. Ferguson, H. E. Gove, A. E. Litherland and R. Batchelor, Bull. Am. Phys. Soc. Series II, **5** (1960) 45.

emitted charged particles. The energy of each charged particle is then converted into a light output using a reasonable law relating the two quantities and the total light output for each incident neutron is obtained by simple addition. To calculate the pulse height distribution this procedure is repeated for about $10^5$ neutrons.

Some experimental measurements with incident neutrons of 0.96, 3.99 and 13.95 MeV have been made to compare with the results of these calculations. Two different methods have been used to ensure that electron pulses from $\gamma$-ray interactions were not observed. First pulse shape discrimination was applied to the output pulse using a circuit previously described by Batchelor *et al.*[7]). Secondly, the scintillator was set up as the detector in a time of flight spectrometer and the incident neutrons and $\gamma$-rays distinguished by their different flight times from a pulsed source.

As a further check on the calculations, the efficiency of the scintillator has been measured relative to a calibrated long counter in the region up to 4 MeV.

Some previous work of this nature has been reported by Hardy[8]), Swartz and Owen[3]) and Broek and Anderson[9]). However, it has been usual to consider only two neutron collisions within the scintillator and hence the calculations are applicable only to scintillators of small dimensions. Hardy[8]) considered the case of a scintillator of thickness 2″, but he encountered difficulty in explaining the observed pulse height distribution. He noted that the calculations did not reproduce a rise at low proton energy in the experimental distribution. Broek and Anderson give details of a method of obtaining a neutron spectrum from an observed pulse height distribution.

In the present work, full details of the neutron interactions are taken into account. As expected this procedure leads to good agreement between theory and experiment.

## 2. Monte Carlo Calculations

The calculations to be described have been made for the geometrical arrangement shown in fig. 1, in which a uniform parallel beam of neutrons is incident on the curved surface of the cylindrical detector. The scintillating liquid has a density of 0.88 g/cc and can be considered to consist of a mixture of hydrogen and carbon atoms in the ratio 1.21 : 1. The liquid is contained in a cylindrical glass

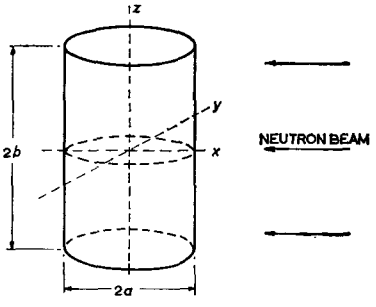


Fig. 1. Geometry of scintillator.

container, the presence of which is ignored in these calculations. The starting co-ordinates of a neutron are defined as

$$x = a\sqrt{1-\xi_1^2} \tag{1}$$

$$y = a\xi_1 \tag{2}$$

$$z = b\xi_2 \tag{3}$$

where $a$ is the radius and b the half height of the cylinder and $\xi_1$, $\xi_2$ are random numbers uniformly distributed in the range 0, 1). Because of symmetry this representation reproduces a uniform beam of neutrons, with each neutron having direction cosines (— 1, 0, 0). The probability distribution of neutron path length, $\rho$, within the scintillator is given in terms of the neutron mean free path, $\lambda$, in the scintillator material by the equation

$$P(\rho)\,\mathrm{d}\rho = \frac{1}{\lambda}\exp\left(-\frac{\rho}{\lambda}\right)\mathrm{d}\rho \quad (0 \leqslant \rho < \infty)\,. \tag{4}$$

It can be easily shown that $\rho = -\lambda \log \xi_3$ is a random deviate from this distribution, $\xi_3$ being a third random number uniform in (0, 1).

By comparing $\rho$ with the thickness of scintillator as seen by the neutron $(2a\sqrt{1-\xi_1^2})$, a decision is

[7]) R. Batchelor, W. B. Gilboy, A. D. Purnell and J. H. Towle, Nucl. Instr. and Meth. 8 (1960) 146.

[8]) J. E. Hardy, Rev. Sci. Instr. 29 (1958) 705.

[9]) H. W. Broek and C. E. Anderson, Rev. Sci. Instr. 31 (1960) 1063.

[10]) E. D. Pendlebury, to be published.

made as to whether this particular neutron escaped without collision, thereby making no contribution to the output, or whether an interaction took place. If a collision occurs, i.e. $\rho < 2a\sqrt{1-\xi^2_1}$, the nuclear data, pertinent to neutron collisions with hydrogen and carbon, are consulted and the energy and direction of the emergent neutron (if any), together with the energy deposited, $E_d$, are computed. The track is then continued, as before, and the process repeated until the neutron escapes or is absorbed or is moderated to thermal energy.

The nuclear data are stored in the machine in a suitable form for consultation by a special subroutine which has generalised inbuilt collision routines and is independent of the main Monte Carlo tracking and analysis programme.

Details of the nuclear data for many elements, including hydrogen and carbon, used at A.W.R.E. will shortly be published[10]), Published experimental cross-sections are used, where available, otherwise the values are based on nuclear theory, or interpolation and extrapolation of the experimental points. The data are converted into punched card form and processed in a special manner[11]) to yield partial cross-sections in each of 128 energy groups extending from 0.025 eV up to 14 MeV. For inelastic events, scattering is assumed to be isotropic in the laboratory system. Elastic scattering by hydrogen is taken to be isotropic in the centre of mass system, but use is made of the measured angular distributions for carbon[12]). Each distribution is assumed to be valid over a certain range of incident neutron energy and is simulated by 32 discrete scatter angle cosines, previously determined in such a manner that random sampling from these 32 members is a correct $\delta$-function representation of the angular distribution in the laboratory system. The corresponding energy reduction factor is precomputed for each of the 32 discrete cosines, thus eliminating the need for extra calculation during the Monte Carlo tracking at the expense of extra storage space.

Table 1 shows a list of all the neutron interactions with hydrogen and carbon which have been introduced into the calculations. Into the third column of this table are entered the charged particles, emitted in these reactions, which have been

TABLE 1
Neutron interactions in the scintillator considered in the Monte Carlo calculations

| Material | Type of reaction introduced into the Monte Carlo calculations | Charged particle considered in computing light output |
|---|---|---|
| H | Elastic scatter | Proton |
| | (n, $\gamma$) | — |
| C | Elastic scatter | Carbon recoil |
| | $C^{12}(n,\alpha)Be^9$ | $\alpha$-particle |
| | $C^{12}(n,n')C^{12*}(3\alpha)$ | — |
| | $C^{12}(n,n')C^{12*}$ | — |
| | $C^{12}(n,\alpha)Be^{9*}(n)Be^8(2\alpha)$ | — |

taken into account in computing the final light output. To simplify the calculations, the light outputs due to reactions with carbon leading to the emission of three $\alpha$-particles have been neglected. Similarly no account has been taken of any $\gamma$-rays emitted in the nuclear reactions. These assumptions are justified in view of the low probabilities of the processes involved.

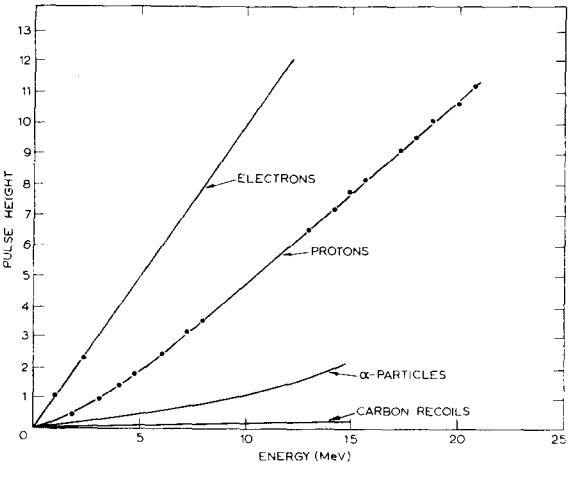


Fig. 2. Relationships between light output and energy for electrons, protons, $\alpha$-particles and carbon recoils, used in the Monte Carlo calculations. The dots are experimental points.

[11]) K. Parker and J. B. Parker, A.W.R.E. (Aldermaston) Report No. 0–20/60 (1960).

[12]) D. J. Hughes and R. S. Carter, B.N.L. Report No. 400 (1956).

For ease of computation the following simple simple relationships between light output (L) and energy of the particle have been used and are plotted in fig. 2.

Protons

$$L_p = 0.215E_p + 0.028E_p^2 \ (0 < E_p < 8 \text{ MeV}) \quad (5a)$$

$$= 0.60E_p - 1.28 \qquad (8 < E_p < 14 \text{ MeV}). \quad (5b)$$

$\alpha$-particles

$$L_\alpha = 0.046\,E_\alpha + 0.007E_\alpha^2 . \quad (6)$$

Carbon recoils

$$L_C = 0.017\,E_C . \quad (7)$$

Prior to this investigation, there was no experimental information on the response of the NE213 liquid scintillator to the various particles. The response for protons (eqs. (5a) and (5b)) was obtained experimentally by the method described in section 4.2.

To obtain eqs. (6) and (7), a calculation of the response to $\alpha$-particles and carbon ions was first performed using the formula due to Birks[13]).

$$\frac{dL}{dE} = \left(1 + kB\frac{dE}{dx}\right)^{-1} \quad (8)$$

where $dE/dx$ is the energy lost by the particle per unit distance travelled in the scintillator. A value of 0.01 g cm$^{-2}$ MeV$^{-1}$ was used for $kB$, which is that found by Evans and Bellamy[14]) for the plastic phosphor NE102. It was found that these curves could be fitted quite well with the expressions (6) and (7). It is obvious that the dominant contribution to the light output arises from the effect of protons and hence the use of the approximate expressions (6) and (7) is not likely to lead to large final errors.

Edge effects, due to the finite ranges of the charged particles, are negligible in the scintillators of sizes considered here, even for neutrons up to 14 MeV.

## 3. Results of the Calculations

Histograms of the various light output distributions are shown in figs. 3–7. Table 2 gives the data from which these curves are drawn. The number of

[13]) J. B. Birks, Proc. Phys. Soc. A **164** (1951) 10.

[14]) H. C. Evans and R. H. Bellamy, Proc. Phys. Soc. **74** (1959) 483.

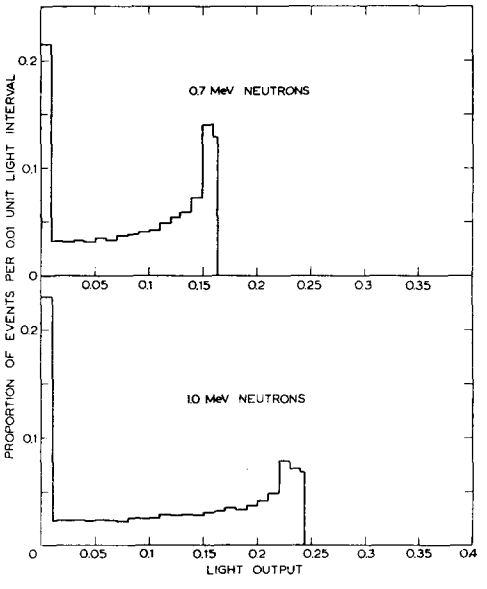


Fig. 3. Theoretical pulse height distributions for 0.7 MeV and 1.0 MeV neutrons, 2″ × 2½é scintillator.

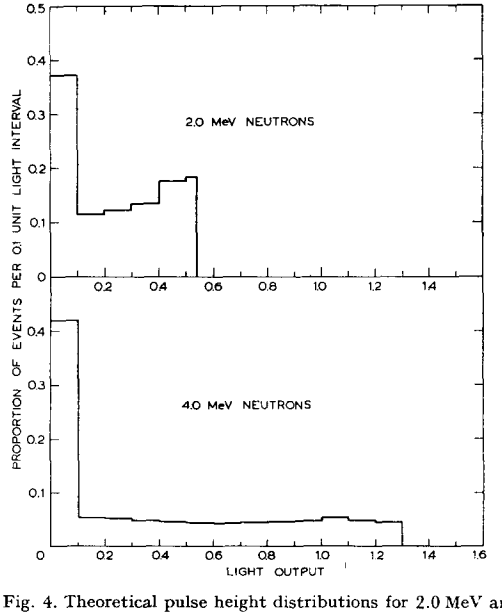


Fig. 4. Theoretical pulse height distributions for 2.0 MeV and 4 MeV neutrons, 2″ × 2½″ scintillator.

TABLE 2

Light output distributions for neutrons of various energies interacting in the scintillators

| Light output interval | Proportion of events | | | Light output interval | Proportion of events | | | Light output interval | Proportion of events | |
|---|---|---|---|---|---|---|---|---|---|---|
| | 2″ × 2½″, 0.7 MeV | 2″ × 2½″, 1.0 MeV | 2″ × 2½″, 2 MeV | | 2″ × 2½″, 4 MeV | 3″ × 4″, 4 MeV | 2″ × 2½″, 8 MeV | | 2″ × 2½″, 14 MeV | 3″ × 4″, 14 MeV |
| 0 –0.01 | 0.2147 | 0.2298 | 0.2528 | 0 –0.1 | 0.4202 | 0.3489 | 0.3917 | 0 –0.1 | 0.4335 | 0.4052 |
| 0.01–0.02 | 0.0310 | 0.0228 | 0.0225 | 0.1–0.2 | 0.0553 | 0.0559 | 0.0486 | 0.1–0.2 | 0.0261 | 0.0336 |
| 0.02–0.03 | 0.0312 | 0.0228 | 0.0123 | 0.2–0.3 | 0.0518 | 0.0531 | 0.0324 | 0.2–0.3 | 0.0234 | 0.0324 |
| 0.03–0.04 | 0.0335 | 0.0230 | 0.0128 | 0.3–0.4 | 0.0484 | 0.0505 | 0.0247 | 0.3–0.4 | 0.0147 | 0.0170 |
| 0.04–0.05 | 0.0318 | 0.0216 | 0.0119 | 0.4–0.5 | 0.0468 | 0.0496 | 0.0243 | 0.4–0.5 | 0.0144 | 0.0191 |
| 0.05–0.06 | 0.0344 | 0.0235 | 0.0123 | 0.5–0.6 | 0.0458 | 0.0510 | 0.0224 | 0.5–0.6 | 0.0570 | 0.0602 |
| 0.06–0.07 | 0.0339 | 0.0231 | 0.0129 | 0.6–0.7 | 0.0448 | 0.0512 | 0.0207 | 0.6–0.7 | 0.0101 | 0.0101 |
| 0.07–0.08 | 0.0374 | 0.0225 | 0.0118 | 0.7–0.8 | 0.0440 | 0.0533 | 0.0204 | 0.7–0.8 | 0.0115 | 0.0118 |
| 0.08–0.09 | 0.0382 | 0.0248 | 0.0117 | 0.8–0.9 | 0.0473 | 0.0554 | 0.0203 | 0.8–0.9 | 0.0100 | 0.0117 |
| 0.09–0.10 | 0.0402 | 0.0242 | 0.0120 | 0.9–1.0 | 0.0487 | 0.0546 | 0.0191 | 0.9–1.0 | 0.0091 | 0.0093 |
| 0.10–0.11 | 0.0432 | 0.0262 | 0.0124 | 1.0–1.1 | 0.0537 | 0.0656 | 0.0188 | 1.0–1.1 | 0.0095 | 0.0103 |
| 0.11–0.12 | 0.0492 | 0.0276 | 0.0110 | 1.1–1.2 | 0.0460 | 0.0538 | 0.0166 | 1.1–1.2 | 0.0090 | 0.0098 |
| 0.12–0.13 | 0.0549 | 0.0268 | 0.0124 | 1.2–1.3 | 0.0438 | 0.0526 | 0.0169 | 1.2–1.6 | 0.0292 | 0.0328 |
| 0.13–0.14 | 0.0590 | 0.0276 | 0.0117 | 1.3–1.4 | 0.0034 | 0.0045 | 0.0152 | 1.6–2.0 | 0.0270 | 0.0280 |
| 0.14–0.15 | 0.0734 | 0.0278 | 0.0126 | 1.4–1.5 | | | 0.0159 | 2.0–2.4 | 0.0274 | 0.0255 |
| 0.15–0.16 | 0.1402 | 0.0307 | 0.0116 | 1.5–1.6 | | | 0.0163 | 2.4–2.8 | 0.0246 | 0.0225 |
| 0.16–0.17 | 0.0538 | 0.0313 | 0.0107 | 1.6–1.7 | | | 0.0154 | 2.8–3.2 | 0.0208 | 0.0220 |
| 0.17–0.18 | | 0.0349 | 0.0116 | 1.7–1.8 | | | 0.0155 | 3.2–3.6 | 0.0211 | 0.0213 |
| 0.18–0.19 | | 0.0333 | 0.0114 | 1.8–1.9 | | | 0.0153 | 3.6–4.0 | 0.0237 | 0.0216 |
| 0.19–0.20 | | 0.0361 | 0.0120 | 1.9–2.0 | | | 0.0146 | 4.0–4.4 | 0.0249 | 0.0236 |
| 0.20–0.21 | | 0.0407 | 0.0117 | 2.0–2.1 | | | 0.0155 | 4.4–4.8 | 0.0253 | 0.0252 |
| 0.21–0.22 | | 0.0482 | 0.0121 | 2.1–2.2 | | | 0.0156 | 4.8–5.2 | 0.0245 | 0.0232 |
| 0.22–0.23 | | 0.0794 | 0.0117 | 2.2–2.3 | | | 0.0149 | 5.2–5.6 | 0.0262 | 0.0256 |
| 0.23–0.24 | | 0.0707 | 0.0122 | 2.3–2.4 | | | 0.0141 | 5.6–6.0 | 0.0247 | 0.0280 |
| 0.24–0.25 | | 0.0206 | 0.0112 | 2.4–2.5 | | | 0.0161 | 6.0–6.4 | 0.0254 | 0.0249 |
| 0.25–0.26 | | | 0.0122 | 2.5–2.6 | | | 0.0163 | 6.4–6.8 | 0.0257 | 0.0246 |
| 0.26–0.27 | | | 0.0124 | 2.6–2.7 | | | 0.0155 | 6.8–7.12 | 0.0211 | 0.0203 |
| 0.27–0.28 | | | 00.120 | 2.7–2.8 | | | 0.0143 | | | |
| 0.28–0.29 | | | 0.0129 | 2.8–2.9 | | | 0.0133 | | | |
| 0.29–0.30 | | | 0.0120 | 2.9–3.0 | | | 0.0144 | | | |
| 0.30–0.31 | | | 0.0120 | 3.0–3.1 | | | 0.0135 | | | |
| 0.31–0.32 | | | 0.0123 | 3.1–3.2 | | | 0.0125 | | | |
| 0.32–0.33 | | | 0.0122 | 3.2–3.3 | | | 0.0122 | | | |
| 0.33–0.34 | | | 0.0143 | 3.3–3.4 | | | 0.0127 | | | |
| 0.34–0.35 | | | 0.0132 | 3.4–3.5 | | | 0.0124 | | | |
| 0.35–0.36 | | | 0.0128 | 3.5–3.6 | | | 0.0016 | | | |
| 0.36–0.37 | | | 0.0137 | | | | | | | |
| 0.37–0.38 | | | 0.0139 | | | | | | | |
| 0.38–0.39 | | | 0.0130 | | | | | | | |
| 0.39–0.40 | | | 0.0125 | | | | | | | |
| 0.40–0.41 | | | 0.0140 | | | | | | | |
| 0.41–0.42 | | | 0.0152 | | | | | | | |
| 0.42–0.43 | | | 0.0155 | | | | | | | |
| 0.43–0.44 | | | 0.0163 | | | | | | | |
| 0.44–0.45 | | | 0.0161 | | | | | | | |
| 0.45–0.46 | | | 0.0170 | | | | | | | |
| 0.46–0.47 | | | 0.0203 | | | | | | | |
| 0.47–0.48 | | | 0.0219 | | | | | | | |
| 0.48–0.49 | | | 0.0245 | | | | | | | |
| 0.49–0.50 | | | 0.0205 | | | | | | | |
| 0.50–0.51 | | | 0.0180 | | | | | | | |
| 0.51–0.52 | | | 0.0181 | | | | | | | |
| 0.52–0.53 | | | 0.0182 | | | | | | | |
| 0.53–0.54 | | | 0.0196 | | | | | | | |
| 0.54–0.55 | | | 0.0036 | | | | | | | |

neutrons tracked was 50000 per run, except for the 8 and 14 MeV runs on the 2″ × 2½″ scintillator; 100000 neutrons were tracked in these cases. On the average each run took about ¾ hour. The statistical errors on the ordinates are less than 10%.

An interesting feature of these histograms is that as the incident neutron energy increases, there is a shift of pulses from high to low light output. This can be understood in the following way. Multiple neutron scattering in the scintillator tends to give large output pulses whereas the non-linear response of the scintillator to protons concentrates the pulses in the region of low output. For incident neutrons of low energy the proportion of multiple scattered events is relatively high and is sufficient to dominate the pulse output distribution. On the other hand, at high energies multiple scattering is not so important and the non-linear pulse height response is the dominant factor affecting the distribution. All the histograms show a large number of very low light pulses and these are due to the recoiling carbon nuclei. Another point of interest is the narrow peak in the light interval 0.5 to 0.6 in the 14 MeV distributions (figs. 5 and 6). This peak is due to the α-particles emitted in the reaction $C^{12}(n, \alpha)Be^{9}$.

Table 3 gives the percentage of neutrons which pass through the scintillator without interacting, the percentage which though interacting, fail to contribute to the light output (due e.g. to $C^{12}(n, n')$) and the total theoretical efficiency. The standard deviations of these results are less than 0.2%. From the theoretical distributions for the 2″ × 2½″ scintillator, the counting efficiencies for various bias levels have been calculated, and are plotted as a function of neutron energy in fig. 8. The bias levels quoted refer to proton energy deposited in the scintillator and hence can be regarded as the minimum neutron energy to which the detector is sensitive. The lines drawn in fig. 8 are smooth curves through the points. If the calculations were to be performed at closely spaced neutron energies, then the curve for zero bias is not expected to be smooth, due to the effect of resonances in the carbon cross-section. Also shown in fig. 8 is a curve for zero bias calculated from the simple formula.

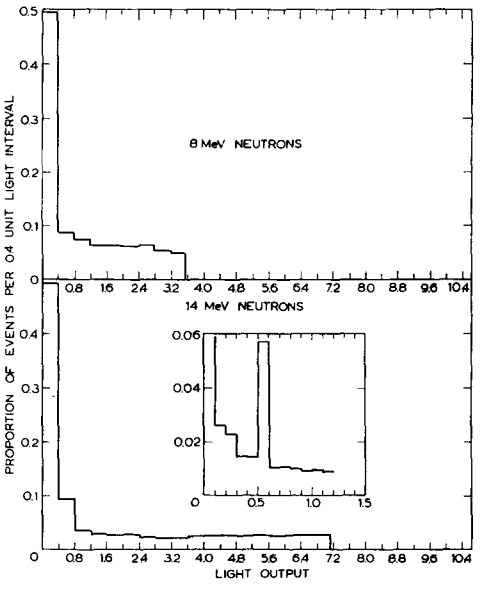


Fig. 5. Theoretical pulse height distributions for 8.0 MeV and 14 MeV neutrons, 2″ × 2½″ scintillator.

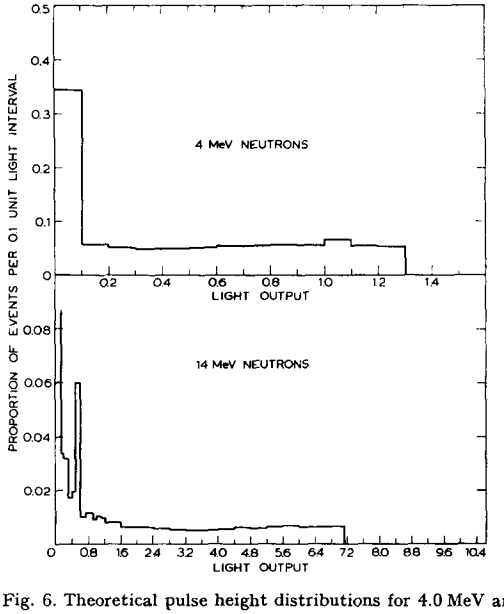


Fig. 6. Theoretical pulse height distributions for 4.0 MeV and 14.0 MeV neutrons, 3″ × 4″ scintillator.

TABLE 3
Details of the numbers of neutrons which interact with the scintillators

| Neutron energy (MeV) | 2″ × 2½″ scintillator | | | 3″ × 4″ scintillator | | |
|---|---|---|---|---|---|---|
| | % uncollided neutrons | % absorbed neutrons† | Efficiency (%) | % uncollided neutrons | % absorbed neutrons† | Efficiency (%) |
| 0.7 | 26.4 | 0 | 73.6 | | | |
| 1.0 | 31.8 | 0 | 68.2 | 19.5 | 0 | 80.5 |
| 2.0 | 44.5 | 0 | 55.5 | | | |
| 4.0 | 53.4 | 0 | 46.6 | 41.2 | 0 | 58.8 |
| 8.0 | 63.8 | 4.5 | 31.7 | | | |
| 14.0 | 71.3 | 4.1 | 24.6 | 61.9 | 4.0 | 34.1 |
| Fission spectrum | 37.9 | 0.1 | 62.0 | 26.2 | 0.1 | 73.7 |

† More precisely: percentage of neutrons which interact but do not contribute to the light output.

$$\text{Efficiency} = (1 - e^{-n_H \sigma_H d}) \qquad (9)$$

where

$n_H$ = number of H atoms per cc of scintillator

$\sigma_H$ = (n, p) cross-section

$d = \frac{1}{2}\pi a$ = mean thickness of scintillator.

This formula is based on the following assumptions.

(a) carbon is not present in the scintillator

(b) the radius of the scintillator is small compared with $1/n_H\sigma_H$.

Swartz and Owen[3]) point out that, in some cases, the efficiency calculated using this formula is approximately equal to that calculated if single hydrogen collisions, single carbon collisions and carbon collisions, followed by hydrogen collisions, are allowed to occur.

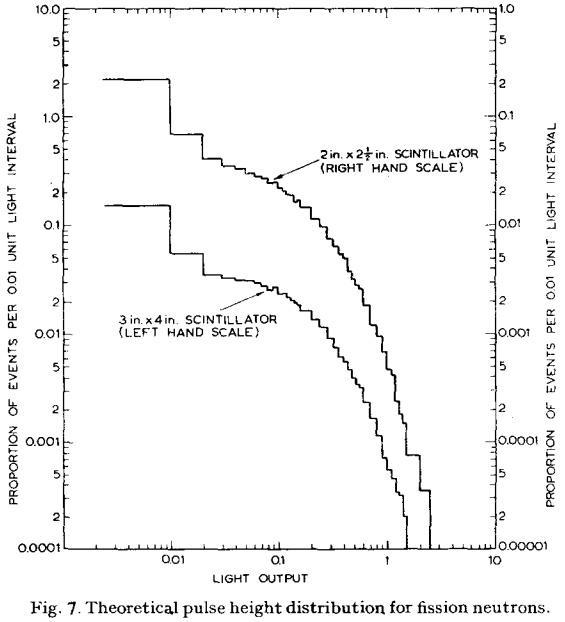


Fig. 7. Theoretical pulse height distribution for fission neutrons.

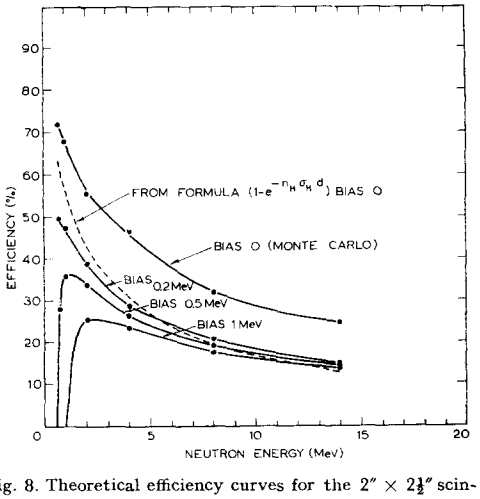


Fig. 8. Theoretical efficiency curves for the 2″ × 2½″ scintillator biassed at various levels. The broken curve represents the efficiency calculated from eq. (9).

## 4. Experimental Measurements

### 4.1. DETECTOR AND EQUIPMENT

The experiments to be described have been carried out with a 2″ diam. × 2½″ long scintillator which is the detector normally used in the time of flight spectrometer for fast neutron studies using the 6 MV Van de Graaff accelerator at Aldermaston. The time of flight apparatus was used in these experiments and since the details have been published elsewhere[15,16]) only a brief description will be given here.

The NE213 liquid is contained in a right cylindrical glass container of wall thickness approximately $\frac{1}{16}$″, and is viewed by two photomultipliers, type 6810A, one optically coupled to each flat end of the cylinder. The outside of the curved surface of the cylinder is coated with white reflecting paint. The complete detector is housed in a brass tube, of wall thickness $\frac{1}{16}$″, and is placed at the centre of a cylindrical shield of water and lead of diameter 4 ft and height 4 ft. Neutrons are incident on the curved surface of the scintillator through a collimating hole of diameter 2½″ in the shield. This means that the sensitive area of the scintillator is not fully exposed to the incident beam, and hence the experimental arrangement does not accurately reproduce the conditions under which the theoretical calculations have been made. This, however, was considered to be relatively unimportant except in the comparison between theoretical and experimental efficiencies. In this case a suitable correction for the loss in sensitive area has been applied. From time of flight spectrum measurements, neutron energy degradation by the collimator is known to be negligible.

The method of applying pulse shape discrimination to the detector is an extension of the method proposed by Owen[2]) and has been previously described in detail[7]). The voltage between the collector and last dynode of one of the photomultipliers (for convenience this will be called the "left" photomultiplier) is restricted to a few volts. The positive swing of the pulse from the last dynode is used to indicate the type of particle which initiated the event. A proton usually gives a larger positive output than an electron and the proton pulse swings positive at a slightly earlier time. This pulse and two linear pulses, one from each photomultiplier, are amplified (differentiating time 3 μsec), passed through voltage discriminators and then applied to a threefold coincidence circuit. Adjustment of the various bias levels and also the coincidence resolving time ensures that the coincidence output signifies the incidence of a neutron. The pulse height distribution appropriate to neutrons is then obtained by gating the linear output of the "right" photomultiplier with this coincidence output. The pulses are analysed on a 100 channel pulse height analyser. If the gating pulse is taken from a twofold coincidence between the two linear outputs, then the resulting pulse distribution is that pertaining to the incidence of both neutrons and γ-rays.

To obtain the pulse distributions by the time of flight method, a pulsed beam is used, the pulse repetition frequency being 5 Mc/sec and the pulse width approximately 2 nanosec. A fast pulse is taken from the "right" photomultiplier and is fed as a start pulse into a time sorter; the stop pulse being obtained from the R.F. which deflects the beam. A twofold coincidence between the two linear pulses from the photomultiplier gates the time sorter output which is observed on a 100-channel pulse height analyser.

The time spectrum exhibits two peaks due to neutrons and two due to γ-rays, superimposed on a small background. To obtain the pulse height distribution appropriate to neutrons, voltage windows are placed across the neutron peaks by means of two single channel analysers. The outputs of the analysers are mixed and arranged to gate the linear output from the "right" photomultiplier and the spectrum is recorded on a second 100 channel pulse height analyser. If the background of the time spectrum is not negligible, a further measurement with the windows set to pass appropriate sections of the background is made. Provided the background is flat, this measurement gives a suitable correction for the background under the neutron peaks.

[15]) R. Batchelor and J. H. Towle, A.W.R.E. (Aldermaston) Report No. NR/P-12/58 (1958).

[16]) B. E. F. Macefield and J. H. Towle, Proc. Soc. A **76** (1960) 56.

### 4.2. MEASUREMENT OF PULSE HEIGHT RESPONSE FOR PROTONS

A necessary preliminary to this work was to establish that the linear output from the "right" photomultiplier was in fact linear, and also to measure the variation of proton pulse height with proton energy for the liquid scintillator. The method adopted was to make some preliminary observations of the pulse height distributions by the pulse shape discrimination method for monokinetic incident neutrons of various energies. In order to extract the required information it was anticipated that the observed distributions would be similar to those predicted by theory but modified at the high energy cut off by resolution. For neutrons in excess of about 2 MeV it was noted that the high energy half of each spectrum is fairly flat and consequently the average pulse height for a proton of energy equal to the incident neutron energy can be taken as the mid point of the fall off of the observed curve. As can be seen from figs. 10 and 12, in the case of 3.99 MeV, this method gives the same result as that obtained by extrapolating the straight line portion of the integral curve to the bias axis.

For these experiments, neutrons in the energy range 13 to 21 MeV were obtained from the T(d, n)$He^4$ reaction, those in the range 4 to 8 MeV from the d(d, n)$He^3$ reaction and those in the range 2 to 4 MeV from the T(p, n)$He^3$ reaction. Gaseous targets were used and the incident particle energy and angle of observation were adjusted to give the desired neutron energy.

The electron response was also measured by observing the Compton edges for the 2.62 MeV thorium $\gamma$-rays and the 1.28 $Na^{22}$ $\gamma$-rays. Periodic measurements with these sources also served to check on the stability of the apparatus.

The results are shown in fig. 2 in which the ordinate scale is chosen to conform with the convention that the electron pulse height is equal to the electron energy. These curves were obtained with an overall H.T. voltage of 1600 applied to the "right" photomultiplier. When this voltage was increased to about 1900 the proton curve showed definite signs of saturation. Reducing the voltage to 1400 produced no change in the shape of the curve, thus indicating that at 1600 V no saturation was occurring. This suggests that the output is linear. It should be noted that no convenient $\gamma$-ray sources exist for a direct check on the linearity in the energy range required.

It is of interest to note that the shape of the measured curve is close to that obtained by Evans and Bellamy[14]) for the plastic phosphor NE102. The slight difference between the two curves can be understood in terms of the different ionisation losses due to the different C:H ratios in the two materials.

### 4.3. MEASUREMENT OF PULSE HEIGHT DISTRIBUTIONS

Measurements have been made by the two methods for incident neutron energies of 3.99 MeV and 13.95 MeV and by the time of flight method only at 0.96 MeV. Details of the neutron sources used and relevant geometrical details are given in table 4.

The results are shown in figs. 9, 10 and 11. In figs. 10 and 11 the results obtained by the two methods are normalised, for illustrative purposes

TABLE 4
Details of the neutron sources and geometry used in the experiment

| | | | |
|---|---|---|---|
| Incident neutron energy | 3.99 MeV | 13.95 MeV | 0.96 MeV |
| Reaction | $H^3$(p,n)$He^3$ | $H^3$(d,n)$He^4$ | $H^3$(p,n)$He^3$ |
| Type of target | Tritium gas | Tritium gas | Tritium gas |
| Energy of bombarding particles | 5.33 MeV | 1.96 MeV | 2.18 MeV |
| Angle of observation relative to incident charged particle beam direction | 30° | 105° | 30° |
| Distance between source and detector | 171 cm | 171 cm | 171 cm |
| Estimated neutron energy spread | 50 keV | 80 keV | 90 keV |

only, so that the areas under the curves are the same. In section 4.4 (see fig. 13) it is shown that the overall detection efficiency is reduced when pulse shape discrimination is applied and consequently the areas under the corresponding curves should be less than the curves obtained by the time of flight method. From fig. 13 we deduce that the rejection rate of proton pulses by the pulse indicator circuit varies with proton energy. This effect is also noticeable in the 13.95 MeV pulse distribution curves (fig. 11) but does not show up at 3.95 MeV (fig. 10). Figs. 10 and 11 are reasonably consistent, however, if the pulse shape discrimination curve of fig. 10 is reduced by about 5% to allow for the reduced efficiency.

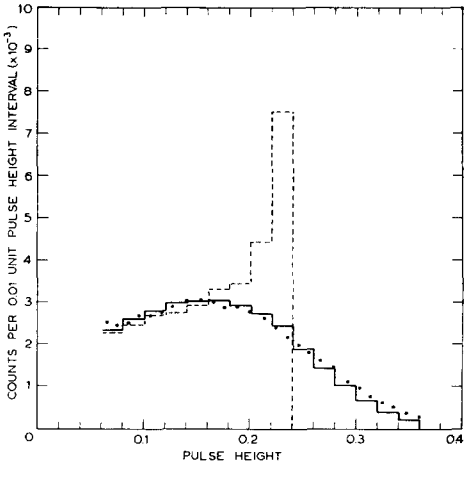


Fig. 9. Pulse height distribution obtained in the 0.96 MeV neutron experiment using the time of flight technique. The dotted line is the theoretical fit without resolution correction; the solid line is the fit with resolution correction.

### 4.4. EFFICIENCY MEASUREMENTS

Measurements of the efficiency of the scintillator with an effective bias of about 200 keV were made in the neutron energy range 0.3 to 3.5 MeV. The $H^3(p, n)He^3$ source, with a gaseous tritium target, was used and the energy of the neutrons incident on the detector was varied by varying the proton energy and the angle of observation relative to the incident proton beam. Angles of 30° and 90° were used, covering the energy ranges 1 to 3.5 MeV and 0.3 to 1.5 MeV respectively. The incident neutron

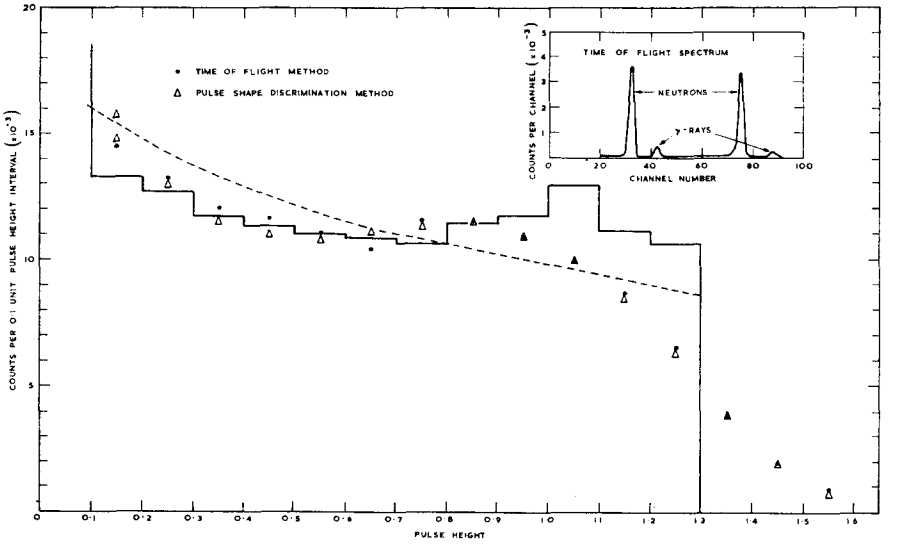


Fig. 10. Pulse height distributions obtained in the 3.99 MeV neutron experiment. The solid line is the fit appropriate to the theory developed in this paper; the dotted line is the theoretical curve based on single collisions with hydrogen. The inset shows the time spectrum of the radiation incident on the scintillator.

flux was measured with a long counter[17]), calibrated with standard neutron sources, placed at the same angle as the scintillator but on the opposite side of the beam piping. The background of from the cell. This background reduces by about a factor 2 when pulse shape discrimination is applied. Under these conditions, a large fraction of the background represents neutrons originating directly

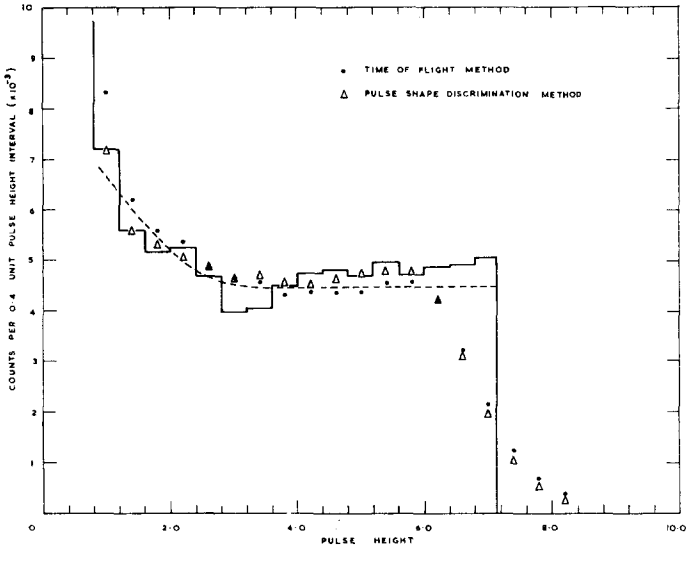


Fig. 11. Pulse height distributions obtained in the 13.95 MeV neutron experiment. The solid line is the fit appropriate to the theory developed in this paper; the dotted line is the theoretical curve based on single collisions with hydrogen.

the long counter from neutrons not directly emitted from the gas cell was measured by placing a shadow cone of paraffin wax approximately midway between the source and counter. A second long counter served to monitor the neutron output.

In this experiment a pulsed beam was used so that at each energy the time spectrum could be observed and the neutron counting rate in the scintillator found by summing the counts in the neutron peaks. Measurements were made with the time sorter output gated by the twofold coincidence between the linear outputs of the photomultipliers and also by the threefold coincidence which introduces the influence of the pulse discriminator circuit.

Apart from the neutron peaks, each time spectrum contains a small fairly flat background which was still present when tritium was removed

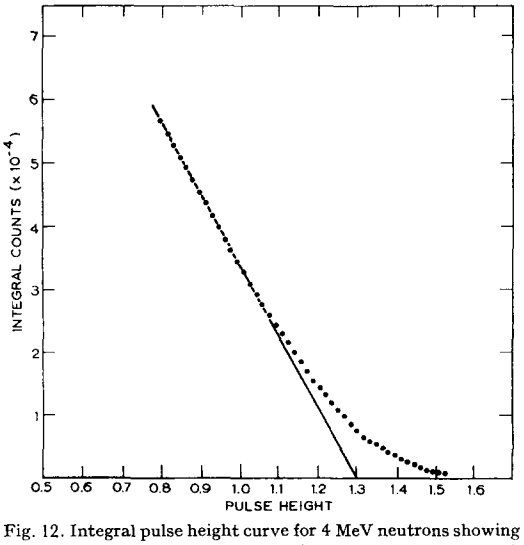


Fig. 12. Integral pulse height curve for 4 MeV neutrons showing the method of extrapolation used to determine the upper cut-off.

[17]) A. O. Hansen and J. L. McKibben, Phys. Rev. **72** (1947) 673.

from interactions between the incident protons and the component parts of the gas cell. Consequently a correction was applied to the long counter rate for the effect of these neutrons since the background

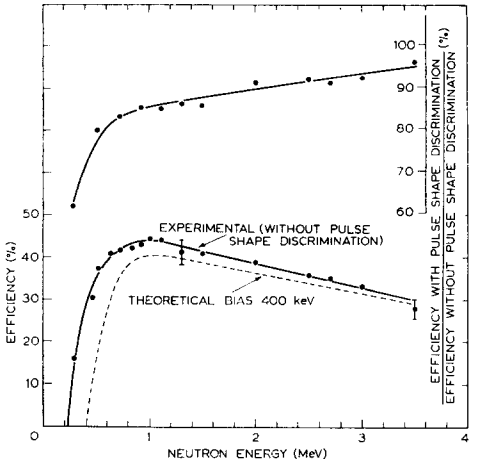


Fig. 13. Results of efficiency measurements and comparison with theory. Upper curve shows the ratio of efficiency obtained with pulse shape discrimination applied to that obtained when this technique is not applied.

measurement with the shadow cone does not include them. The correction factor was taken to be the ratio of the total counts in the time spectra to the counts under the neutron peaks observed with pulse shape discrimination applied. Its magnitude varied from about 2% at 0.5 MeV to 5% at 3 MeV neutron energy. In view of the uncertainties involved in applying the correction and also the accuracy of the long counter calibration, the overall uncertainty in the measured efficiency is about $\pm$ 7%. The final results are shown in fig. 13.

Also plotted in fig. 13 is a curve of the ratio of the efficiency with pulse shape discrimination to that obtained when the technique is not applied.

### 5. Comparison between Theory and Experiment

Theoretical pulse distributions for 1, 4 and 14 MeV are fitted to the experimental curves shown in figs. 9, 10 and 11, respectively. In each case the curves are normalised to the same area. At 4 and 14 MeV the high cut off points of the theoretical curves are made to coincide with the points at which the extrapolated straight lines of the experimental integral curves cut the bias axis. In these cases the agreement between theory and experiment is good provided due allowance is made for the resolution of the detector. (Resolution here is taken to mean the spread in output pulse height for monoenergetic charged particles produced uniformly throughout the scintillator.) For comparison, theoretical curves based on the assumption that only single scatterings with hydrogen can take place are also shown. At 4 MeV there is a marked difference between the two theoretical curves, and experiment gives definite support to the sophisticated theory. This difference is not apparent at 14 MeV presumably because multiple scattering effects are much less important at this energy.

At 1 MeV, resolution is expected to modify considerably the predicted curve. To illustrate this a triangular resolution function has been folded into the theoretical curve. From an inspection of the 4 and 14 MeV results it was estimated that the half width of the resolution function was given approximately by the expression $0.29\,L^{\frac{1}{2}}$. It can be seen in fig. 9 that the modified theoretical curve fits the experimental result extremely well. A curve corresponding to single hydrogen collisions would not show a peak.

A direct comparison between the measured efficiency curve and one of the theoretical curves shown in fig. 8 cannot be made since instrumental resolution is expected to have a large effect, particularly at low energy. Since the efficiency is predicted to be a sensitive function of the bias it is obvious that an accurate resolution correction would be required in order to make a quantitative comparison between theory and experiment. This cannot be done because the necessary detailed information on the resolution at low energies is not known. In view of this the discussion will be restricted to a few qualitative remarks.

Resolution will affect the theoretical curves shown in fig. 8 in the following way. The effective bias will be lowered and the efficiency will be increased at all energies. However, as the energy is increased, the percentage increase in efficiency will become smaller. In fig. 13 a theoretical curve for

bias 400 keV is shown along with the experimental results. It can be seen that resolution will modify this curve to produce one which is qualitatively consistent with the experimental curve.

## 6. Conclusions

This study has shown that the line shapes from organic scintillators, having dimensions of a few inches, are well understood and can be calculated by the Monte Carlo programme described. The programme does not include a correction for resolution. The programme also permits the calculation of detector efficiency, but because of uncertainties in applying a resolution correction, and because the efficiency is critically dependent on bias at low energies, and with low bias applied, the calculations can be in serious error at low energy. At high energies and with a bias exceeding say 1 MeV the efficiency changes only slowly with bias and hence the theoretical efficiency, as calculated from table 2 is considered to be quite accurate. In passing, it is worth mentioning that the measurement of efficiency becomes progressively more difficult with increasing neutron energy (apart from 14 MeV). As a general rule, therefore, it is advisable to measure the efficiency at low energies and calculate it at high energies, say above 3 MeV.

Care should be taken in applying the results to a detector which has a technique of pulse shape discrimination applied since this usually eliminates some proton pulses as well as electron pulses. In this connection, a study of the rejection rate of the proton pulses by the circuit used would be of considerable interest.

## Acknowledgement

The assistance of Mr. A. D. Purnell in this work is gratefully acknowledged.